NIH Public Access
Author Manuscript
J Proteome Res. Author manuscript; available in PMC 2014 October 04.

Published in final edited form as:
J Proteome Res. 2013 October 4; 12(10): 4435–4448. doi:10.1021/pr400466x.

Vesicular trafficking and stress response coupled to PI3K inhibition by LY294002 as revealed by proteomic and cell biological analysis

Tomáš Takáč[1], **Tibor Pechan**[2], **Olga Šamajová**[1], and **Jozef Šamaj**[1,*]

[1]Centre of the Region Haná for Biotechnological and Agricultural Research, Department of Cell Biology, Faculty of Science, Palacký University, Šlechtitelů 11, CZ-783 71 Olomouc, Czech Republic

[2]Institute for Genomics, Biocomputing & Biotechnology, Mississippi State University, MS 39762, USA

Abstract

LY294002 is a synthetic quercetin-like compound which, unlike wortmannin, is an inhibitor of phosphatidylinositol 3-kinase (PI3K). It inhibits endocytosis and vacuolar transport. We report here on the proteome-wide effects of LY294002 on *Arabidopsis* roots focusing on proteins involved in vesicular trafficking and stress response. At the subcellular level, LY294002 caused swelling and clustering of late endosomes leading to inhibition of vacuolar transport. At the proteome level, this compound caused changes in abundances of proteins categorized to 10 functional classes. Among proteins involved in vesicular trafficking, a small GTPase ARFA1f was more abundant, indicating its possible contribution to the aggregation and fusion of late endosomes triggered by LY294002. Our study provides new information on storage proteins and vacuolar hydrolases in vegetative tissues treated by LY294002. Vacuolar hydrolases were downregulated while storage proteins were more abundant, suggesting that storage proteins were protected from degradation in swollen multivesicular bodies upon LY294002 treatment. Upregulation of 2S albumin was validated by immunoblotting and immunolabelling analyses. Our study also pointed to the control of antioxidant enzyme machinery by PI3K because LY294002 downregulated two isozymes of superoxide dismutase. This most likely occurred via PI3K–mediated downregulation of protein AtDJ1A. Finally, we discuss specificity differences of LY294002 and wortmannin against PI3K which are reflected at the proteome level. Compared to wortmannin, LY294002 showed more narrow and perhaps also more specific effects on proteins as suggested by gene ontology functional annotation.

Keywords

LY294002; proteomics; storage proteins; *Arabidopsis*; roots; antioxidant enzymes; vesicular trafficking

[*]**Corresponding author:** Prof. Dr. Jozef Šamaj, Centre of the Region Haná for Biotechnological and Agricultural Research, Faculty of Science, Palacký University, Šlechtitelů 11, 783 71 Olomouc, Czech Republic, jozef.samaj@upol.cz, Web: http://www.cr-hana.eu/cellbiol, phone:+420585634978.

Supporting information

Supporting Information Available: This material is available free of charge via the Internet at http://pubs.acs.org."

NIH-PA Author Manuscript
NIH-PA Author Manuscript
NIH-PA Author Manuscript

NIH-PA Author Manuscript
NIH-PA Author Manuscript
NIH-PA Author Manuscript

Introduction

Phosphatidylinositol (PI) signaling delivers multiple stress or developmental signals and thus modulates subcellular and physiological processes, such as vesicular trafficking, stress response and cell/organ development.[1]

Phosphatidylinositol 3 phosphate (PI3P) and phosphatidylinositol 4 phosphate (PI4P) are principal components of PI signaling, which are produced by phosphatidylinositol 3-kinase (PI3K) and PI4 kinases (PI4Ks). Products of these kinases recruit PI3P and PI4P–binding proteins to the membranes,[2] and mediate membrane fusion and trafficking events in the cell. Most frequently, two inhibitors of PI3/4Ks are applied in studies investigating PI signaling, namely wortmannin and LY294002 (2-(4-morpholinyl)-8-phenyl-4H-1-benzopyran-4-one). While wortmannin inhibits PI3K and PI4Ks in a concentration dependent manner,[3,4] LY294002 is accepted as a more selective inhibitor of PI3K.[5,6] It was reported that LY294002 inhibits also PI3K independent proteins such as mTOR and CK2.[7,8] Targeted proteomic screen for identification of new LY294002 targets by using immobilized LY294002 analogue on sepharose beads and subsequent identification of bound proteins derived from mammalian cell lines revealed possible novel targets such as aldehyde dehydrogenase 2, fructosamine 3-kinase, ketosamine 3-kinase, galactokinase, phosphofructokinase and pyridoxal kinase.[9]

LY294002 is a synthetic compound based on quercetin. Currently, LY294002 represents a valuable tool for studies of vacuolar trafficking and endocytosis in plants. Like wortmannin, it competes for ATP binding site of PI3K[10] and binds to Lys-833 residue. It inhibits PI3K with an IC_{50} value (concentration required for 50% inhibition) of 0.43 μg/ml (1.40 μM) irrespective of the phosphorylation state of the enzyme.[5]

At the subcellular level, LY294002 blocks endocytosis and vacuolar trafficking in similar manner to wortmannin. LY294002 inhibits the internalization of sucrose[11] in plant heterotrophic cells. Vacuole-targeted sporamin-GFP fusion protein accumulates in the cytosolic punctuate structures in the presence of both wortmannin and LY294002 in *Arabidopsis* protoplasts.[12] However, there are also some differences between the effects of wortmannin and LY294002. Unlike wortmannin, LY294002 does not inhibit the early stages of endocytosis (as measured by uptake of the styryl dye FM 1–43), while negatively affecting the fusion of late endosomes with tonoplast in *Arabidopsis* root hairs.[13] In another study, wortmannin completely abolished staining and reduced the number of endosomes visualized by FYVE-DsRed in transiently transformed detached leaves of *Nicothiana benthamiana*, while in LY294002-treated leaves, these endosomes occasionally remained, but their motility was reduced.[14] It remains unknown, whether these differences could be related to different specificities of wortmannin and LY29002 towards PI3K and PI4K.

In physiological response, LY294002 (100μM) promotes stomatal opening, and inhibits stomatal closing induced by abscisic acid.[15] LY294002 inhibits polar tip-growth of root hairs, probably by decreasing reactive-oxygen species (ROS) levels, but does not affect root hair initiation.[13] Pretreatment with LY294002 also blocked auxin-mediated ROS generation and reduced the sensitivity of roots to gravistimulation.[16] While the amount of PI3P increased in response to auxin, this effect was abolished by pretreatment with LY294002.[16]

Recently, a combined proteomic and cell biological study provided an important survey on the effects of wortmannin on *Arabidopsis* roots.[4] Cell biological approaches validated proteomic data on RabA1d, a small Rab GTPase localized to early endosomes, and downregulated by fusion of early endosomes with late endosomes after wortmannin treatment. These results demonstrated the feasibility of combined proteomic and cell

NIH-PA Author Manuscript

NIH-PA Author Manuscript

NIH-PA Author Manuscript

biological methods to study physiological changes in *Arabidopsis* roots caused by pharmacological perturbation of PI3/4K signaling.

In this study, we performed a proteomic analysis of *Arabidopsis* roots using a more specific inhibitor of PI3K, namely LY294002. We aimed to integrate proteomic data with the subcellular effects (e.g. on endosomes and antioxidant activity) caused by this inhibitor in root cells. Inhibitor effects at subcellular level were validated by live-cell imaging, and proteomic data on upregulation of 2S albumin were validated by both immunoblots and immunolabelling on intact roots. Most obvious similarities and differences between previously reported wortmannin effects and LY294002 are discussed.

Experimental procedures

Plant material and cultivation

Seeds of *Arabidopsis thaliana* (ecotype Col-0 and transgenic Col-0 lines with PI3P and endosomal molecular markers) were surface sterilized and placed on half-strength MS culture medium (pH 5.7) containing 1% (w/v) sucrose and 0.8% (w/v) phytagel. The plates were stored at 4°C for 48 h to break dormancy, and then kept vertically under 16 h light/8 h dark, 22°C conditions, for 10 days (proteomic analysis) or 6 days (microscopic analysis).

Seedlings were surface-treated with liquid ½ MS media containing 33 μM LY294002 (Sigma) dissolved in dimethylsulfoxide (DMSO; final concentration 0.3% DMSO [v/v]) for 2 h, while preventing complete submergence of the roots in the liquid. Control plants were treated with solution containing ½ MS medium supplemented with 0.3% DMSO. Roots were quickly dissected and harvested for protein extraction.

The development of transgenic *Arabidopsis* lines used for microscopic analysis was described previously.[17] As *in vivo* PI3P marker, and late endosomes marker we have used line stably expressing the GFP-tagged double FYVE construct, and line expressing YFP-tagged RabF2a,[17] respectively.

Proteomic analysis

Protein extraction for two-dimensional electrophoresis and 2-D LC-MS/MS— Proteins were extracted according to the protocol of Takáč et al.[18] Briefly, roots were frozen in liquid nitrogen and homogenized to a fine powder using a mortar and pestle. Phenol was used for total protein extraction according to a modified method of Hurkmann and Tanaka.[19] A detailed description of the protein extraction method is provided in the supplemental data.

Two-dimensional electrophoresis—The 2-DE was performed as published in our previous study.[18] Details are provided in supplemental data. Extracts from plant material harvested from three independent biological experiments (3 biological replicates) were used for analysis. The gels were stained by Bio-Safe Coomassie brilliant blue staining solution (Bio-Rad) according to the manufacturer's instructions. Gels were scanned using a densitometer (GS-800, Bio-Rad) and analyzed using the program PD-Quest 8.0 (Bio-Rad). The spot intensities were normalized according to total density in the gel images. After automated spot detection and matching, manual editing was carried out to ensure correct matches. One-way ANOVA statistical analysis was performed with a 95% significance level to determine differentially abundant proteins (LY294002-treated vs. control samples). Spots showing statistically significant ($p \leq 0.05$) abundance differences were selected and manually picked for digestion and identification.

NIH-PA Author Manuscript

NIH-PA Author Manuscript

NIH-PA Author Manuscript

Trypsin digestion and mass spectrometry—Trypsin digestion was performed as described by Hajduch et al. [20] The peptide mix was extracted from gel plugs using 100 μL of extraction solution (60% [v/v] acetonitrile, 1% [v/v] formic acid), and spotted onto an anchor chip target (Bruker Daltonics) using the dried droplet method.[21] We used α-Cyano-4-hydroxycinnamic acid (2 mg/ml in 50% ACN and 0.2% TFA) as a matrix. Mass spectrometry analysis was performed using a MALDI-TOF-TOF (Ultraflex II, Bruker Daltonics) according to Takáč et al.[18]

MS-mode acquisition (1000–4000 Da) consisted of 150 laser shots averaged from 5 sample positions. From each full scan, the top 10 peaks were used for subsequent MS/MS analysis. Peptide fragmentation was performed using collision induced dissociation and 250 laser shots from 5 sample positions were summed up for each parent ion. Data processing of raw spectra was performed using Bruker software (Flex analysis 2.4 and BioTools 3.1).

Mascot search (Mascot Server 2.2.03,) was conducted using an MS tolerance of 50 ppm, and an MS/MS tolerance of 800 mmu (milli mass units).

One miscleavage was allowed. Carbamidomethylation was chosen as fixed modification, while oxidation (H, W, M) and phosphorylation (S, T, Y) were used as variable modifications. The data were matched against the *Arabidopsis* genus taxonomy UniProt database, which contained 31,856 entries as of 01/12/2011.

Standard scoring (MOWSE score = 60) and a significance threshold of $p<0.05$ for protein/peptide identification were chosen for filtering Mascot results. These parameters and values are applied according to well established consensus.

Preparation of protein samples for 2-D LC-MS/MS—The protocol used for in-solution trypsin digestion of proteins was adapted from the method described by Donaldson et al.[22] Briefly, the protein precipitate was resuspended in 50μl of 6 M urea. Prior to digestion, a total amount of 100 μg protein was subjected to reduction by addition of 10 μl of 50 mM DTT (incubated at 70°C for 30 minutes), followed by alkylation with 11μl of 100 mM iodoacetamide (incubated at room temperature for 1 h). Finally, an additional 10 μl of 50 mM DTT was added to the protein solution.

Urea concentration was lowered to 1 M by addition of Milli-Q water. Proteins were digested with 20 μl of trypsin (0.1μg/μl) at 37°C overnight. The digestion was stopped by the addition of 4 μl of 1% formic acid. Next, the peptides were desalted using SEP PAK light C18 columns (Waters) according to the manufacturer's instructions. The eluted peptides were vacuum-dried to produce a pellet, stored at −80°C, and re-dissolved in 20 μl of 0.1% formic acid, 5% ACN just prior to the 2-D LC/MSMS analysis.

2-D LC-MS/MS analysis—The liquid chromatography - mass spectrometry analysis was performed using the ProteomeX Workstation (Thermo). It consists of a Surveyor auto sampler and a Surveyor HPLC unit coupled directly in line with a LCQ Deca XP Plus – ESI ion trap mass spectrometer controlled by XCALIBUR 1.4 SR1 software (Thermo). The raw data were collected as published previously.[23] Detailed method parameters are provided in the supplemental data.

The HPLC step consisted of a 2-D LC separation on a strong cation exchange (SCX) column (SCX BioBasic 0.32 × 100 mm) followed by reverse phase column (BioBasic C18, 0.18 × 100 mm; Thermo Hypersil-Keystone). A flow rate of 3μl/min was used for both SCX and reverse phase columns. For SCX, salt steps of 0, 10, 15, 25, 30, 35, 40, 45, 50, 57, 64, 90, and 700 mM ammonium acetate in 5% v/v ACN and 0.1% v/v formic acid were applied.

NIH-PA Author Manuscript

NIH-PA Author Manuscript

NIH-PA Author Manuscript

The reverse phase column was eluted by ACN gradient (in 0.1% v/v formic acid) as follows: 5%-30% for 30 min, 30%-65% for 9 min, 95% for 5 min, 5% for 15 min, for a total of 59 min elution and data collection for each of thirteen salt steps. The mass spectrometer was programmed to operate in the data dependent mode with dynamic exclusion and four scan events: one MS scan (m/z range: 300–1700) and three MSMS scans of the three most intense ionized species detected in MS scan in real time.

Protein identification and label-free quantification—The triplicate raw files containing the MS and MSMS data for each biological sample were searched using the TurboSEQUEST algorithm of the Bioworks Browser 3.2 EF2 (Thermo) software as described previously.[18] Cysteine carbamidomethylation and methionine oxidation were included in the search criteria. The data were matched against both target and decoy databases. The NCBI (www.ncbi.nlm.nih.gov) *Arabidopsis* genus taxonomy referenced protein database (31,856 entries as of December 2011) served as the target database, while its reversed copy served as a decoy database. The unfiltered TurboSEQUEST result (.srf) files were subjected to further validation, statistical and spectral counting based label-free quantitative analysis utilizing the ProteoIQ 2.3.02 (Bioinquire) software. The crucial parameters were set as follows: minimum peptide length = 5 amino acids (AAs), maximum protein false discovery rate (FDR) = 5%, minimum protein group probability = 95%, (the graphs justifying these parameter values as properly chosen and stringent for high confidence protein identification can be found in the supplemental data, Figure S1). Only the "Top" proteins (as defined by ProteoIQ - within a protein group, each and every respective peptide could be matched to the top protein) were further considered. Normalization was based on total sampling (spectral count) in biological groups and replicates. A minimum of five spectral counts per protein were required for quantitation. Spectral counts related to both unmodified and modified peptides were considered. The MSMS method included dynamic exclusion with repeat counts = 2, repeat duration = 0.5 minute and exclusion duration = 2.0 minutes. One-way ANOVA statistical analysis was performed and only the proteins with $p \leq 0.05$ were reported as differentially expressed. Identifications based on single peptides were accepted only if supported by multiple spectral counts. Pertinent peptide and protein identification details, including annotated spectral images are available in supplemental data.

Live cell imaging

For microscopy, 5 day old plants were transferred to micro-chambers between microscopic slides and cover slips with one Parafilm layer as a spacer. The chambers were filled with liquid half-strength MS medium. In order to perform drug treatments, LY294002 at a final concentration of 33μM in the culture medium was infiltrated into the chambers by perfusion and plants were incubated for 2 h. As controls, plants were incubated with a control solution containing ½ MS medium supplemented with 0.3% DMSO. Microscopic analysis was performed using a Zeiss LSM 710 confocal laser scanning microscope (Carl Zeiss Jena, Germany). All images were acquired using a 40x objective lens with numerical aperture 1.42. GFP was excited at 488nm and detected between 500–535 nm, YFP was excited at 514 nm and detected between 518–540 nm. Post-processing of images was done with the aid of Zeiss ZEN software (Ver.2010b), Image J 1.38x, Photoshop 6.0/CS and Microsoft PowerPoint applications.

Whole-mount immunofluorescence labeling

Six day old whole seedlings were labeled according to method of Sauer et al.[24] with small modification: prior to fixation, seedlings were treated either with 33μM LY294002 or with 0,3% DMSO in ½ liquid MS medium for 2h; seedlings were fixed in 1.5% paraformaldehyde and 0.5% glutaraldehyde in ½ MTSB buffer (50mM K-PIPES, 5mM

NIH-PA Author Manuscript

NIH-PA Author Manuscript

NIH-PA Author Manuscript

$MgSO_4x7H_20$, 5mM EGTA) at pH 6.8; cell wall digestion enzyme mixture contained 1% meicelase, 1% cellulase and 1% macerozyne in PBS; samples were incubated with rabbit anti-*Arabidopsis* 2S albumin (At2S2) primary antibody diluted 1:200 in PBS supplemented with 2% BSA at 4°C overnight and subsequently with secondary antibody Alexa-Fluor 488 goat anti-rabbit IgG (H+L) (Invitrogen) diluted 1:500 in PBS containing 2% BSA) for 3h (1.5 h at 37°C and 1.5 h at room temperature). Microscopic analysis of immunolabeled samples was performed using a Zeiss LSM710. Alexa488-conjugated antibody was excited at 488 nm and fluorescence was detected between 500 and 535 nm. The post-processing of images was done using ZEN 2010 software, Photoshop 6.0/CS and Microsoft PowerPoint.

Immunoblot analysis

For protein extraction, roots were homogenized in ice cold RIPA extraction buffer (50mM Tris/HCl pH 8, 150mM NaCl, 1% NP-40, 0.5% sodium deoxycholate and 0.1% SDS) supplemented with SDS sample buffer (in final concentration of 40% glycerol, 240 mM Tris/HCl pH 6.8, 8% SDS, 0.04% bromophenol blue, 5% beta-mercaptoethanol), boiled and subsequently centrifuged at 14000g at 4°C for 15 min.

Protein extracts were separated by SDS-PAGE (MINI-Protean II cell system, Biorad). Identical protein concentrations were loaded for each sample. Proteins were transferred to a polyvinylidene difluoride (PVDF) membrane (GE Healthcare) in a wet tank unit (Bio-Rad) at 100 V using the transfer buffer for 1.5 h.[25] For immuno-detection of protein bands, the membrane was blocked with 3% (w/v) bovine serum albumin (BSA) and 3% (w/v) non-fat dry milk powder in Tris-buffer-saline (TBS, 100 mM Tris-HCl; 1.5 mM NaCl; pH 7.4) for 1 hour, and subsequently incubated with a primary antibody against *Arabidopsis* 2S albumin (At2S2[22]) diluted 1:2000 in TBS-T (TBS; 0.1% Tween 20) containing 1% [w/v] BSA at room temperature for 1.5 h or at 4°C overnight. After washing in TBS-T, the membrane was incubated at room temperature for 1.5 h with a horseradish peroxidase conjugated goat anti-rabbit IgG secondary antibody (Santa Cruz Biotechnology, sc-2004), diluted 1:5000 in TBS-T containing 1% [w/v] BSA. Following at least six washing steps, proteins were detected by incubating the membrane in freshly prepared enhanced chemiluminescence (ECL) reagent for 2 min. ECL reagent was prepared using the following solutions: 1 ml of solution A (200 ml 0.1M Tris-HCl (pH 8.6); 50 mg Luminol (Sigma-Aldrich)), 100 µl of solution B (11 mg para-Hydroxycoumarin acid (Sigma-Aldrich) in 10 ml DMSO and 0.3 µl H_2O_2 (37%). Luminescence was detected using Chemidoc MP documentation system (Biorad).

Isozyme analysis

Samples were homogenized using liquid nitrogen in 1 mM EDTA containing 50 mM sodium phosphate buffer (pH 7.8). Subsequently, the extract was centrifuged at 12,000 g and the supernatant was desalted and concentrated on Amicon Ultra Ultracel-10 K membrane (Millipore) centrifugation columns (14,000 g, 4 °C, 15 min). The isozymes were separated on 10% native PAGE. In the case of SOD, samples were loaded on two separate gels. Prior to SOD isozyme visualization, one of the gels was pre-incubated in 0.05% hydrogen peroxide (in 50 mM Na phosphate buffer, pH 7.8) to inhibit Cu/Zn SOD. Afterward, the gels were stained by dark two-step incubation in solution containing 0.6 mM NBT in 50 mM Na-phosphate buffer (pH 7.8) followed by incubation in solution containing 0.06 mM riboflavin, 5 mM EDTA and 0.25% TEMED. Finally, the gels were exposed to light until the SOD activity appeared as negative bands. The isozymes of glutathione peroxidase were visualized according to Lin et al.[27] by pre-incubation in solution containing 50mM Tris-HCl pH 8, 13mM GSH and 0.004% H_2O_2 and subsequent signal development in solution of 50mM Tris-HCl pH 8, 1.2 mM 3-(4,5-dimethylthiazol-2-yl)-2,5-diphenyltetrazolium bromide (MTT) and 1.6 mM phenazine methosulfate. Peroxidase isozymes were stained by

NIH-PA Author Manuscript

NIH-PA Author Manuscript

NIH-PA Author Manuscript

incubation in solution containing 50mM Na phosphate (pH7.0), 0.05% of 4-Cl-1-naftol and 20μl of 30% H_2O_2.

Results

The effects of LY294002 at the subcellular level

Since LY294002 inhibits PI3K, an enzyme responsible for PI3P formation,[6] we have used stably transformed *Arabidopsis* plants carrying 2xFYVE-GFP construct.[17] This is a molecular marker visualizing specifically PI3P, which can be used to investigate effects of LY294002 on the subcellular distribution of PI3P–positive endosomes (Figure 1A and B). We have found swelling and clustering of endosomes visualized by 2xFYVE-GFP construct (Figure 1C and D). Using YFP-RabF2a as a reliable marker for late endosomes[17] (Figure 1 E and F) a very similar swelling and clustering of endosomes caused by LY294002 was observed (Figure 1G and H).

These results suggest obvious physiological effects of LY294002 on vesicular trafficking at the subcellular level resulting in inhibition of vacuolar transport and aggregation of late endosomes. Such affects are at least partially similar to those induced by wortmannin.[4]

Effects of LY294002 on Arabidopsis root proteome

Employing combined gel-based (Figure 2) and gel-free proteomic approaches we detected 73 (18 and 55, respectively) differentially abundant proteins after LY294002 treatment of *Arabidopsis* roots. All 73 proteins are listed in Table 1 and classified into 10 functional categories in Figure 3. Out of them, metabolic proteins were most affected by LY294002, and they represented 36% of differentially abundant proteins. Malate dehydrogenase was the most upregulated protein (9.3 fold) while AtArd2 (acireductone dioxygenase 1) was the most downregulated one (0.26 fold) upon treatment with LY294002. Stress-related proteins represented the second most affected functional class of proteins (18%). They were followed by proteins associated with protein synthesis (17%). LY294002 also affected vesicular trafficking proteins (7%), as well as proteins involved in proteolysis (6%), protein folding (4%) and storage (4%), nucleic acid binding (3%) and in cell division (1%). Fourteen proteins were identified as unique in LY294002-treated samples, while three proteins were present only in controls. Due to the limitation in MS based quantitative methods, this should not be viewed as absolute, but it offers a strong indication of protein abundance. More detailed classification according to KEGG pathway database (http://www.genome.jp/kegg/pathway.html; [28]) is presented in Table S1. An overview of functional networks affected by LY294002 in *Arabidopsis* roots is shown in Figure 4. This analysis showed that two clusters of translation-related and metabolic proteins possessed multiple interacting protein nodes which were affected by LY294002.

LY294002 targets vacuolar hydrolases, storage proteins and proteins localized to trans-Golgi network

LY29402 affected several proteins involved in endomembrane trafficking. Among them, it decreased the abundance of small GTPase RabA1d, which is localized to *trans*-Golgi network (TGN).[29] Recently, RabA1d was reported to be downregulated by wortmannin due to the fusion of TGN vesicles with late endosomes.[4] Next, an ADP-ribosylation factor A1F (ARFA1F) was affected by LY294002. ARFs are, similarly to RabA1d, small GTPases cycling between active (GTP-bound) and inactive (GDP-bound) state, and they recruit cytosolic coat proteins to sites of vesicle budding and fusion.[30] Upregulation of ARFA1F in response to LY294002 indicates its possible accumulation to ensure clustering and fusion of late endosomes.

NIH-PA Author Manuscript

NIH-PA Author Manuscript

NIH-PA Author Manuscript

We also detected a significant downregulation of vacuolar hydrolases such as aleurain-like protease and cathepsin B-like cysteine protease. These proteins are known to be transported to the vacuole via TGN vesicles and late endosomes/multivesicular bodies (MVBs).[31]

Downregulation of vacuolar hydrolases by LY294002 (inhibiting vesicular transport to the vacuole) suggests that turnover of these proteins is likely altered and shifted towards preferential degradation. This might be a part of the feedback mechanism to LY294002-inhibited vesicular transport of hydrolases to the vacuole. On the other hand, the storage proteins cruciferin 3; cruciferin 2 and 2S albumin were detected by 2D LC MS/MS only in LY294002 treated sample suggesting their intracellular accumulation under such conditions. To validate this result by independent method, we performed immunoblot analysis using an antibody against *Arabidopsis* 2S albumin[26] (Figure 5A). Immunoblot experiments revealed that 2S albumin was significantly more abundant upon LY294002 treatment as revealed also by quantitation of band densities presented in Figure 5B. Further, we performed immunolocalization experiments to study the effect of LY294002 on subcellular distribution and relocation of 2S albumin. In control root cells, this protein was localized to distinct punctate structures (Figure 5C, D) resembling late endosomes visualized by RabF2a molecular marker. LY294002 caused swelling and clustering of these spot-like structures (Figure 5E, F) accompanied by a general increase of the fluorescent signal. It was further strengthened by quantification of the size of these punctate structures (Figure 5G). These measurements documented that the diameter of vesicles containing 2S albumin was mostly in the range of 0.2–0.6 μm in control cells (roughly corresponding to the size of endosomes in *Arabidopsis*) while it increased up to 2 μm in cells treated by LY294002. Thus, punctate endosome-like structures labeled by antibody against 2S albumin showed similar subcellular redistribution, including swelling and aggregation, as previously described for molecular markers specific for PI3P and late endosomes (Figure 1).

LY294002 substantially modified stress response proteins and the antioxidant enzyme machinery

LY294002 also affected the proteins involved in enzymatic antioxidant defense as revealed by our proteomic screen. Two isozymes of superoxide dismutase, namely Cu/Zn SOD2 (CSD2) and Fe SOD1, were downregulated by LY294002. In order to strengthen these data we performed functional isozyme spectra analysis using native PAGE followed by SOD activity staining. In agreement with proteomic data, Cu/Zn SOD isozyme showed decreased activity in response to LY294002 treatment (Figure 6A, Table 2). The identity of this isozyme was proved on the basis of its sensitivity to H_2O_2. These results suggest decreased capacity to remove superoxide anion after PI3K inhibition by LY294002 but also points to decreased hydrogen peroxide formation via SOD activity. Despite limited hydrogen peroxide production suggested by lower SOD activity, hydrogen peroxide decomposing enzymes, such as catalase 2, secretory peroxidase 39 and glutathione peroxidase 6 were upregulated by LY294002. Notably, the abundance of glutathione peroxidase 6, which uses glutathione to remove hydrogen peroxide, was more than four-fold higher in LY294002 treated *Arabidopsis* roots as compared to the control. Similar increase was also observed in GPX activity as revealed by staining of native PAGE gels (Figure 6B, band with Rm 0.08, Table 2). Furthermore, three isozymes of peroxidases stained on native PAGE gels showed increased activity after LY294002 treatment in agreement with proteomic data (Figure 6C). These results point to the PI3K–dependent control over antioxidant enzyme machinery in *Arabidopsis* roots.

Additionally, LY294002 strongly suppressed the abundance of other stress-related proteins such as C2H2-like zinc finger protein and low-molecular-weight cysteine-rich 68 protease

NIH-PA Author Manuscript

NIH-PA Author Manuscript

NIH-PA Author Manuscript

inhibitor. Finally, the CSD1 interacting protein class I glutamine amidotransferase domain-containing protein, also named DJ1A[32] was also downregulated by LY294002.

Discussion

Together with genetic tools, pharmacological inhibitors such as brefeldin A and wortmannin are widely used in cell biology and physiological studies. They are assumed to be specific for certain subcellular events, depending on their molecular targets, such as ARF-GEF, PI3K and PI4K, respectively. In general, inhibitors are considered to be more useful if their targets are more specific, as is the case of LY294002 inhibiting PI3P but not PI4P. Most importantly, pharmacological treatments combined with large scale proteomic analysis represent a very valuable tool for screening new proteins essential for cell physiological events, especially when proteomic data are validated by cell biological or biochemical methods. In plants, this strategy led to the identification of new proteins regulating dynamics of cytoskeleton, calcium signalling and vesicular trafficking.[4,18,33,34] Moreover, combined exploitation of proteomics and cell biology for elucidation of inhibitor effects revealed that their applications have wider consequences mainly related to physiological changes (e.g. in vesicular trafficking), or modification of biochemical mechanisms (e.g. anti-oxidative system) in *Arabidopsis* roots.[4,18]

In this study, we presented proteome changes in *Arabidopsis* roots affected by PI3K inhibitor LY294002. Proteomic results for selected proteins such as 2S albumin and anti-oxidative enzymes were validated by independent biochemical and cell biological methods. Finally, similarities and differences between proteome-wide effects of wortmannin and LY294002 are discussed.

LY294002 versus wortmannin: overall proteome changes

Sixteen proteins were differentially regulated by both wortmannin and LY294002, but only seven of them were affected in the same manner, e.g. up- or down-regulated. These proteins are listed in Table 3.

There were some differences between LY294002 and wortmannin[4] in several functional classes of differentially regulated proteins in *Arabidopsis* root proteome. These differences could be accounted either to the narrower specificity of the LY294002 towards PI3K in comparison to wortmannin or to possible differences in other PI3/4K–independent targets of these inhibitors.[8,9] For example, wortmannin modified the abundance of proteins involved in signalling (inositol 1,3,4-trisphosphate 5/6-kinase and phospholipase D alpha 1), lipid metabolism (lipoamide dehydrogenase and dihydrolipoamide dehydrogenase 2) and DNA repair (DNA-damage-repair/toleration 2 and histone H3;[4] but these functional classes were not modified by LY294002. Four proteins involved in stress response (Fe superoxide dismutase 1, peroxidase, putative rare cold inducible gene 3 and major latex protein-related) and two enzymes involved in nitrogen metabolism (glutamate dehydrogenase 2 and glutamine synthetase 2) were affected by LY294002 and wortmannin in an opposite manner (Table 3). LY294002 and wortmannin also differently affected the protein folding as suggested by different abundance of luminal binding protein (Table 3).

Further, we compared gene ontology functional annotations (annotations were assigned by BLAST2Go bioinformatics tool[35] using TAIR GO database) of differentially regulated proteins after LY294002 and wortmannin treatments. Concerning biological processes, LY294002 affected less functional groups compared to wortmannin (Figure 7A) which might be related to partially different target specificities of both inhibitors. In terms of molecular function we have found marked differences in protein abundances of individual classes between LY294002 and wortmannin (Figure 7B). LY294002 affected a higher

NIH-PA Author Manuscript

NIH-PA Author Manuscript

NIH-PA Author Manuscript

number of proteins belonging to GO “protein binding” and “nucleotide binding” (proteins interacting selectively and non-covalently with a nucleotide), and lower number of proteins of GO transferase activity (proteins catalyzing transfer of a group, e.g. a methyl group, glycosyl group, acyl group, phosphorus-containing), if compared to wortmannin. Tables showing the GO terms and their protein abundances in both aspects of gene ontology annotation (biological process and molecular function) are available in supplemental data.

The protein-protein interaction analysis suggested that LY294002 substantially affected clusters of translational machinery and metabolic proteins in *Arabidopsis* roots. PI3K is known to act upstream to TOR kinase which controls translation in animals and yeasts.[36] This PI3K–mediated regulation of translation has not been described in plants so far. Our results indicate that the translation machinery might function in a PI3K dependent manner, as supported by this and previous study using wortmannin,[4] respectively.

LY294002 and wortmannin show similar subcellular effects on late endosomes in Arabidopsis roots

At the subcellular level, we observed LY294002-induced swelling and clustering of late endosomes labeled by 2xFYVE-GFP and YFP-RAbF2a, as it was found in wortmannin-treated cells previously.[4] Some differences between the subcellular effects of these two compounds on endosome clustering and swelling cannot be ruled out. Nevertheless, it was reported previously that unlike wortmannin [37] , LY294002 did not inhibit early stages of endocytosis (as measured by uptake of the styryl dye FM 1–43) in Arabidopsis root cells.[13] Moreover, LY294002 was less effective in disturbing FYVE-labeled endosomes in detached transiently transformed leaves of *Nicothiana benthamiana*.[14]

Therefore, effects of both inhibitors leading to impaired endosomal trafficking and vacuolar transport are most likely a consequence of PI3K rather than PI4K inhibition. Simultaneously, the physiological changes were accompanied by the downregulation of vacuolar proteases (aleurain-like protease and cathepsin B-like cysteine protease), most probably due to their degradation and attenuated turnover, as a consequence of a treatment by both inhibitors.

Proteomics and cell biology show accumulation of storage proteins in response to blocked vacuolar trafficking by LY294002

Proteomic analysis identified three storage proteins being substantially more abundant upon the treatment with LY294002. Consistently, the immunoblot and immunolabeling analyses showed accumulation and relocation of 2S albumin to aggregated punctate structures resembling late endosomes after LY294002 treatment. Similar effect was observed after wortmannin treatment in *Arabidopsis* cell cultures since 2S albumin-GFP remained in the lumen of enlarged PVCs as shown by CLSM.[31] Notably, the vacuolar transport of storage proteins in vegetative tissues is not well understood. Our results suggest that the degradation of storage proteins is inhibited upon swelling of MVBs after LY294002 treatment, as suggested also by the downregulation of vacuolar proteases such as aleurain-like protease as well as cathepsin B-like cysteine protease. It is consistent with previous reports showing that transport of lytic enzymes and storage proteins to the central vacuole is likely to be mediated by the same VSR-positive PVC/MVB populations in BY-2 and *Arabidopsis* cultured cells,[31] as well as in *Arabidopsis* embryo cells.[38]

ARFA1f is likely involved in vesicular transport towards vacuole in Arabidopsis roots

LY294002 affected the abundances of two small GTPases, namely RabA1d and ARFA1f. ARFA1f was upregulated after LY294002 treatment. In their GTP-bound active state, ARF GTPases recruit coat proteins to patches of specific membranes in order to induce vesicle

NIH-PA Author Manuscript

NIH-PA Author Manuscript

NIH-PA Author Manuscript

budding.[30] ARFA1c, which is closely related to ARFA1f (differs only in one amino acid), was reported to control vacuolar trafficking and also secretion of proteins carrying vacuolar sorting signal (BP80 receptor ligands).[39] This ARF GTPase colocalizes with ARA7, an endosomal Rab GTPase.[40,41]

Our proteomic analysis suggests that ARFA1f could also be involved in vacuolar trafficking in *Arabidopsis* roots, and its upregulation might be related to swelling and aggregation of late endosomes upon treatment with LY294002.

Differently to ARFA1f, TGN-localized RabA1d[29] was downregulated by LY294002. Recently it was shown that RabA1b may be involved in the transport between TGN and plasma membrane, which is likely also the case of closely related RabA1d.[42] Wortmannin decreased the dot-like cytoplasmic signal of RabA1b and it accumulated close to the plasma membrane.[42] Similar distortion of the dot like localization was observed in the case of RabA1d after wortmannin.[4] The downregulation of RabA1d after LY294002 treatment further supports interpretation about TGN depletion after PI3K/PI4K inhibition.[4,43,44]

PI3K possibly regulates the antioxidant enzymatic machinery

It is known that wortmannin and LY294002 suppress the intracellular levels of reactive oxygen species in *Arabidopsis*.[13,37] This occurs as a consequence of decreased activity and expression of NADPH oxidase[37,45] which is responsible for the generation of superoxide radicals and can be reversed mainly by PI3P.[37] Such decreased expression of NADPH oxidase arises from inhibition of Rac-1 GTPase translocation from cytosol to plasma membrane by wortmannin and LY294002.[45] Thus, the production of ROS seems to depend on PI3K. Treatment by LY294002 lowered abundance of two isozymes of SOD in *Arabidopsis* roots in our proteomic screen. These enzymes are decomposing superoxide anion by simultaneous production of hydrogen peroxide. We suggest that decrease in Cu/Zn SOD abundance, as provided by specific activity staining on native PAGE gels, was connected to reduced demand to decompose superoxide radicals which were produced at lower level in the presence of LY294002.[13] Furthermore, LY294002 negatively affected the abundance of class I glutamine amidotransferase domain-containing protein, also named AtDJ1A. This protein, localized to cytoplasm and nucleus, interacts with and activates Cu/Zn SOD in *Arabidopsis*.[32] Therefore, we may suggest that PI3K probably couples the NADPH oxidase endocytosis with DJ1A–mediated downregulation of Cu/ZnSOD.

In conclusion, pharmacological proteomic screen using PI3P inhibitor LY294002 provided valuable information about storage protein processing during blocked vacuolar transport conditions. The subcellular effects of LY294002 were accompanied by changes in abundance of several important proteins related to vesicular trafficking, as summarized in Figure 8. Since vacuolar hydrolases were downregulated while storage proteins were more abundant, this suggested that storage proteins were protected from degradation in swollen multivesicular bodies formed after LY294002 treatment. LY294002 also caused attenuated enzymatic defense against superoxide radicals that might be linked to decreased NADPH oxidase activity. Thus, our study pointed to the new link between PI3K and antioxidant enzyme machinery. Finally, marked differences between wortmannin and LY294002 were found on proteome level, in spite of similarities in subcellular changes of endosomes caused by both inhibitors.

Supplementary Material

Refer to Web version on PubMed Central for supplementary material.

NIH-PA Author Manuscript

NIH-PA Author Manuscript

NIH-PA Author Manuscript

Acknowledgments

This work was supported by grant No. ED0007/01/01 to the Centre of the Region Haná for Biotechnological and Agricultural Research, Faculty of Science, Palacký University, Olomouc, Czech Republic, by Genomics for Southern Crop Stress and Disease, USDA CSREES 2009–34609–20222 and by grant No. NIH INBRE P20GM103476 and by the Operational Program Education for Competitiveness - European Social Fund (project CZ.1.07/2.3.00/20.0165). We thank Prof. Karsten Niehaus and Carola Eck from Bielefeld University for their help and advice during initial stage of this project. Our gratitude goes to Mrs. Linda Breazeale for English grammar editing.

References

1. Munnik T, Vermeer JEM. Osmotic stress-induced phosphoinositide and inositol phosphate signalling in plants. Plant Cell Environ. 2010; 33:655–669. [PubMed: 20429089]
2. Stenmark H, Gillooly DJ. Intracellular trafficking and turnover of phosphatidylinositol 3-phosphate. Seminars in Cell & Developmental Biology. 2001; 12:193–199. [PubMed: 11292385]
3. Matsuoka K, Bassham DC, Raikhel NV, Nakamura K. Different sensitivity to wortmannin of two vacuolar sorting signals indicates the presence of distinct sorting machineries in tobacco cells J. Cell Biol. 1995; 130:1307–1318.
4. Takáč T, Pechan T, Šamajová O, Ovečka M, Richter H, Eck C, Niehaus K, Šamaj J. Wortmannin treatment induces changes in *Arabidopsis* root proteome post-Golgi compartments J. Proteome Res. 2012; 11:3127–3142.
5. Vlahos CJ, Matter WF, Hui KY, Brown RF. A specific inhibitor of phosphatidylinositol 3-kinase, 2-(4-morpholinyl)-8-phenyl-4H-1-benzopyran-4-one (LY294002). J. Biol. Chem. 1994; 269:5241–5248. [PubMed: 8106507]
6. Mueller-Roeber B, Pical C. Inositol phospholipid metabolism in Arabidopsis Characterized and putative isoforms of inositol phospholipid kinase and phosphoinositide-specific phospholipase C. Plant Physiol. 2002; 130:22–46. [PubMed: 12226484]
7. Brunn GJ, Williams J, Sabers C, Wiederrecht G, Lawrence JC, Abraham RT. Direct inhibition of the signaling functions of the mammalian target of rapamycin by the phosphoinositide 3-kinase inhibitors, wortmannin and LY294002. EMBO J. 1996; 15:5256–5267. [PubMed: 8895571]
8. Davies SP, Reddy H, Caivano M, Cohen P. Specificity and mechanism of action of some commonly used protein kinase inhibitors. Biochem J. 2000; 351:95–105. [PubMed: 10998351]
9. Gharbi SI, Zvelebil MJ, Shuttleworth SJ, Hancox T, Saghir N, Timms JF, Waterfield MD. Exploring the specificity of the PI3K family inhibitor LY294002. Biochem. J. 2007; 404:15–21. [PubMed: 17302559]
10. Walker EH, Pacold ME, Perisic O, Stephens L, Hawkins PT, Wymann MP, Williams RL. Structural determinants of phosphoinositide 3-kinase inhibition by wortmannin, LY294002, quercetin, myricetin, and staurosporine. Mol. Cell. 2000; 6:909–919. [PubMed: 11090628]
11. Etxeberria E, Baroja-Fernandez E, Muñoz FJ, Pozueta-Romero J. Sucrose-inducible endocytosis as a mechanism for nutrient uptake in heterotrophic plant cells. Plant Cell Physiol. 2005; 46:474–481. [PubMed: 15695454]
12. Kim DH, Eu YJ, Yoo CM, Kim YW, Pih KT, Jin JB, Kim SJ, Stenmark H, Hwang I. Trafficking of phosphatidylinositol 3-phosphate from the *trans*-Golgi network to the lumen of the central vacuole in plant cells. Plant Cell. 2001; 13:287–301. [PubMed: 11226186]
13. Lee Y, Bak G, Choi Y, Chuang W-I, Cho H-T, Lee Y. Roles of phosphatidylinositol 3-kinase in root hair growth. Plant Physiol. 2008; 147:624–635. [PubMed: 18408046]
14. Bar M, Avni A. EHD2 inhibits ligand-induced endocytosis and signaling of the leucine-rich repeat receptor-like protein LeEix2. Plant J. 2009; 59:600–611. [PubMed: 19392695]
15. Jung J-Y, Kim Y-W, Kwak JM, Hwang J-U, Young J, Schroeder JI, Hwang I, Lee Y. Phosphatidylinositol 3- and 4-phosphate are required for normal stomatal movements. Plant Cell. 2002; 14:2399–2412. [PubMed: 12368494]
16. Joo JH, Yoo HJ, Hwang I, Lee JS, Nam KH, Bae YS. Auxin-induced reactive oxygen species production requires the activation of phosphatidylinositol 3-kinase. FEBS Lett. 2005; 579:1243–1248. [PubMed: 15710420]

NIH-PA Author Manuscript

NIH-PA Author Manuscript

NIH-PA Author Manuscript

17. Voigt B, Timmers ACJ, Šamaj J, Hlavacka A, Ueda T, Preuss M, Nielsen E, Mathur J, Emans N, Stenmark H, Nakano A, Baluska F, Menzel D. Actin-based motility of endosomes is linked to the polar tip growth of root hairs. Eur. J. Cell Biol. 2005; 84:609–621. [PubMed: 16032929]
18. Takáč T, Pechan T, Richter H, Müller J, Eck C, Böhm N, Obert B, Ren H, Niehaus K, Šamaj J. Proteomics on brefeldin A-treated *Arabidopsis* roots reveals profilin 2 as a new protein involved in the cross-talk between vesicular trafficking and the actin cytoskeleton. J. Proteome Res. 2011; 10:488–501. [PubMed: 21090759]
19. Hurkman WJ, Tanaka CK. Solubilization of plant membrane proteins for analysis by two-dimensional gel electrophoresis. Plant Physiol. 1986; 81:802–806. [PubMed: 16664906]
20. Hajduch M, Ganapathy A, Stein JW, Thelen JJ. A systematic proteomic study of seed filling in soybean Establishment of high-resolution two-dimensional reference maps, expression profiles, and an interactive proteome database. Plant Physiol. 2005; 137:1397–1419. [PubMed: 15824287]
21. Karas M, Hillenkamp F. Laser desorption ionization of proteins with molecular masses exceeding 10,000 daltons. Anal. Chem. 1988; 60:2299–2301. [PubMed: 3239801]
22. Donaldson JR, Nanduri B, Burgess SC, Lawrence ML. Comparative proteomic analysis of *Listeria monocytogenes* strains F2365 and EGD. Appl. Environ. Microbiol. 2009; 75:366–373. [PubMed: 19028911]
23. Nanduri B, Lawrence ML, Vanguri S, Pechan T, Burgess SC. Proteomic analysis using an unfinished bacterial genome: the effects of subminimum inhibitory concentrations of antibiotics on *Mannheimia haemolytica* virulence factor expression. Proteomics. 2005; 5:4852–4863. [PubMed: 16247735]
24. Sauer M, Paciorek T, Benková E, Friml J. Immunocytochemical techniques for whole-mount in situ protein localization in plants. Nat Protoc. 2006; 1:98–103. [PubMed: 17406218]
25. Towbin H, Staehelin T, Gordon J. Electrophoretic transfer of proteins from polyacrylamide gels to nitrocellulose sheets: procedure, some applications. Proc. Natl. Acad Sci U.S.A. 1979; 76:4350–4354. [PubMed: 388439]
26. Shimada T, Yamada K, Kataoka M, Nakaune S, Koumoto Y, Kuroyanagi M, Tabata S, Kato T, Shinozaki K, Seki M, Kobayashi M, Kondo M, Nishimura M, Hara-Nishimura I. Vacuolar processing enzymes are essential for proper processing of seed storage proteins in *Arabidopsis thaliana* . J. Biol. Chem. 2003; 278:32292–32299. [PubMed: 12799370]
27. Lin C-L, Chen H-J, Hou W-C. Activity staining of glutathione peroxidase after electrophoresis on native and sodium dodecyl sulfate polyacrylamide gels. Electrophoresis. 2002; 23:513–516. [PubMed: 11870757]
28. Kanehisa M, Goto S, Sato Y, Furumichi M, Tanabe M. KEGG for integration and interpretation of large-scale molecular data sets. Nucleic Acids Res. 2012; 40:D109–D114. [PubMed: 22080510]
29. Ovečka M, Berson T, Beck M, Derksen J, Šamaj J, Baluška F, Lichtscheidl IK. Structural sterols are involved in both the initiation and tip growth of root hairs in *Arabidopsis thaliana* . Plant Cell. 2010; 22:2999–3019. [PubMed: 20841426]
30. Vernoud V, Horton AC, Yang Z, Nielsen E. Analysis of the small GTPase gene superfamily of *Arabidopsis* . Plant Physiol. 2003; 131:1191–1208. [PubMed: 12644670]
31. Miao Y, Li KY, Li H-Y, Yao X, Jiang L. The vacuolar transport of aleurain-GFP and 2S albumin-GFP fusions is mediated by the same pre-vacuolar compartments in tobacco BY-2 and *Arabidopsis* suspension cultured cells. Plant J. 2008; 56:824–839. [PubMed: 18680561]
32. Xu XM, Møller SG. ROS removal by DJ-1. Plant Signal Behav. 2010; 5:1034–1036. [PubMed: 20671441]
33. Chen Y, Chen T, Shen S, Zheng M, Guo Y, Lin J, Baluška F, Šamaj J. Differential display proteomic analysis of *Picea meyeri* pollen germination and pollen-tube growth after inhibition of actin polymerization by latrunculin B. Plant J. 2006; 47:174–195. [PubMed: 16771841]
34. Wu X, Chen T, Zheng M, Chen Y, Teng N, Šamaj J, Baluška F, Lin J. Integrative proteomic cytological analysis of the effects of extracellular Ca(2+) influx on *Pinus bungeana* pollen tube development. J Proteome Res. 2008; 7:4299–4312. [PubMed: 18715029]
35. Conesa A, Götz S, García-Gómez JM, Terol J, Talón M, Robles M. Blast2GO: a universal tool for annotation, visualization and analysis in functional genomics research. Bioinformatics. 2005; 21:3674–3676. [PubMed: 16081474]

NIH-PA Author Manuscript

NIH-PA Author Manuscript

NIH-PA Author Manuscript

36. Robaglia C, Thomas M, Meyer C. Sensing nutrient energy status by SnRK1 and TOR kinases. Curr. Opin. Plant Biol. 2012; 15:301–307. [PubMed: 22305521]

37. Leshem Y, Seri L, Levine A. Induction of phosphatidylinositol 3-kinase-mediated endocytosis by salt stress leads to intracellular production of reactive oxygen species and salt tolerance. Plant J. 2007; 51:185–197. [PubMed: 17521408]

38. Otegui MS, Herder R, Schulze J, Jung R, Staehelin LA. The proteolytic processing of seed storage proteins in *Arabidopsis* embryo cells starts in the multivesicular bodies. Plant Cell. 2006; 18:2567–2581. [PubMed: 17012602]

39. Pimpl P, Hanton SL, Taylor JP, Pinto-daSilva LL, Denecke J. The GTPase ARF1p controls the sequence-specific vacuolar sorting route to the lytic vacuole. Plant Cell. 2003; 15:1242–1256. [PubMed: 12724547]

40. Xu J, Scheres B. Cell polarity: ROPing the ends together. Curr Opin Plant Biol. 2005; 8:613–618. [PubMed: 16182602]

41. Böhlenius H, Mørch SM, Godfrey D, Nielsen ME, Thordal-Christensen H. The Multivesicular Body-Localized GTPase ARFA1b/1c Is Important for Callose Deposition and ROR2 Syntaxin-Dependent Preinvasive Basal Defense in Barley. Plant Cell. 2010; 22:3831–3844. [PubMed: 21057060]

42. Asaoka R, Uemura T, Ito J, Fujimoto M, Ito E, Ueda T, Nakano A. Arabidopsis RABA1 GTPases are involved in transport between the *trans*-Golgi network and the plasma membrane, and are required for salinity stress tolerance. Plant J. 2013; 73:240–249.

43. Wang J, Cai Y, Miao Y, Lam SK, Jiang L. Wortmannin induces homotypic fusion of plant prevacuolar compartments. J. Exp. Bot. 2009; 60:3075–3083. [PubMed: 19436047]

44. Scheuring D, Viotti C, Krüger F, Künzl F, Sturm S, Bubeck J, Hillmer S, Frigerio L, Robinson DG, Pimpl P, Schumacher K. Multivesicular bodies mature from the *trans*-Golgi network/early endosome in *Arabidopsis* . Plant Cell. 2011; 23:3463–3481. [PubMed: 21934143]

45. Liu J, Zhou J, Xing D. Phosphatidylinositol 3-kinase plays a vital role in regulation of rice seed vigor via altering NADPH oxidase activity. PLoS ONE. 2012; 7:e33817. [PubMed: 22448275]

NIH-PA Author Manuscript
NIH-PA Author Manuscript
NIH-PA Author Manuscript

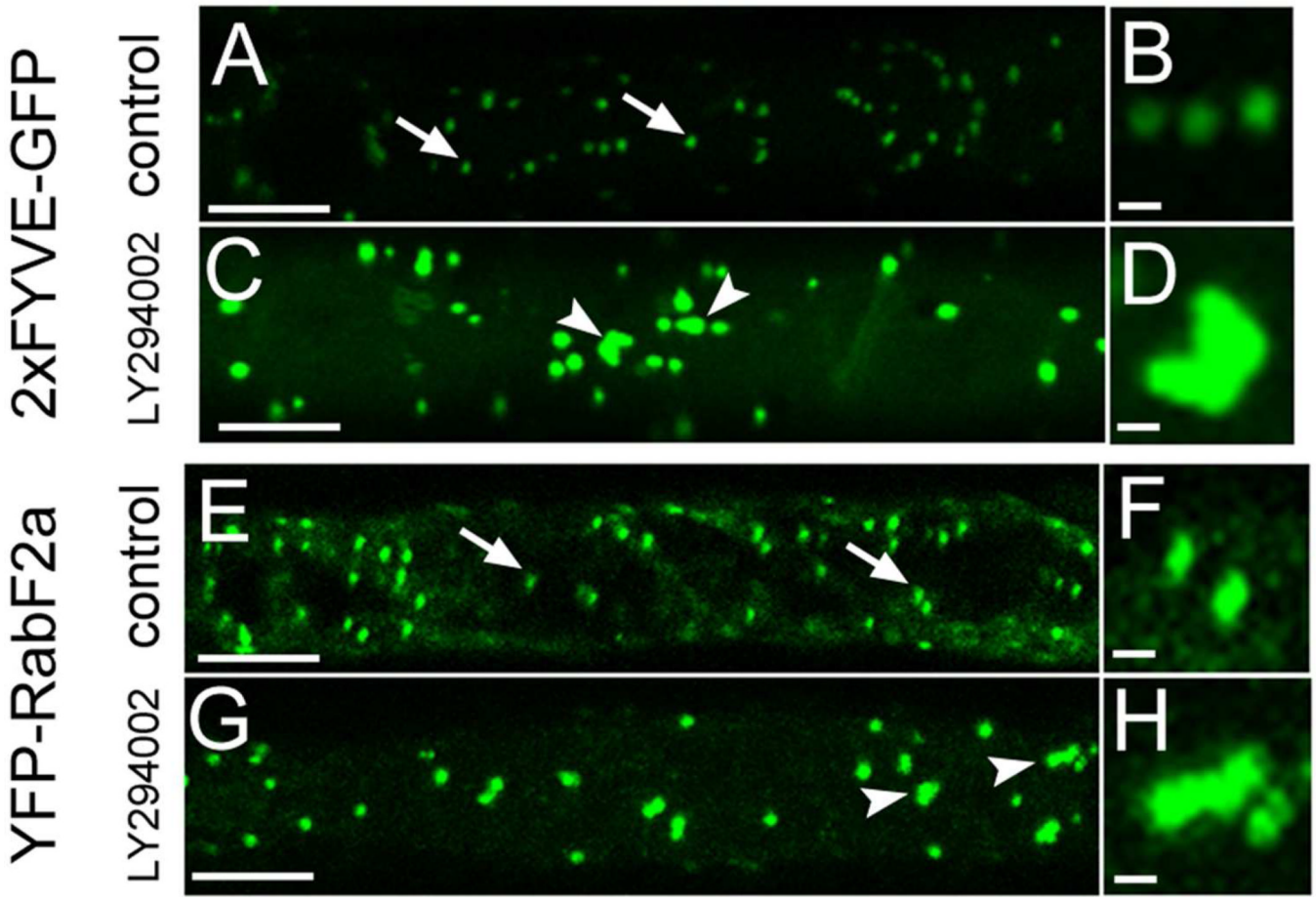

Figure 1.

Subcellular redistribution of late endosomes containing PI3P (as visualized by 2xFYVE-GFP marker, A-D) and RabF2a–YFP molecular marker (E-H) in Arabidopsis root cells treated with 33 μM LY294002 for 2 h. Microscopic visualization of PI3P and RabF2a in individual late endosomes of control cells as indicated by arrows in A, B, E and F. Treatment with LY294002 caused swelling and association of late endosomes in treated cells (indicated by arrowheads in C, D, G, H) as visualized by PI3P marker 2xFYVE-GFP (A-D) and endosomal marker YFP-RabF2a (E-H). Bars represent 10 μm for A, C, E, G, and 1 μm for B, D, F, H.

NIH-PA Author Manuscript

NIH-PA Author Manuscript

NIH-PA Author Manuscript

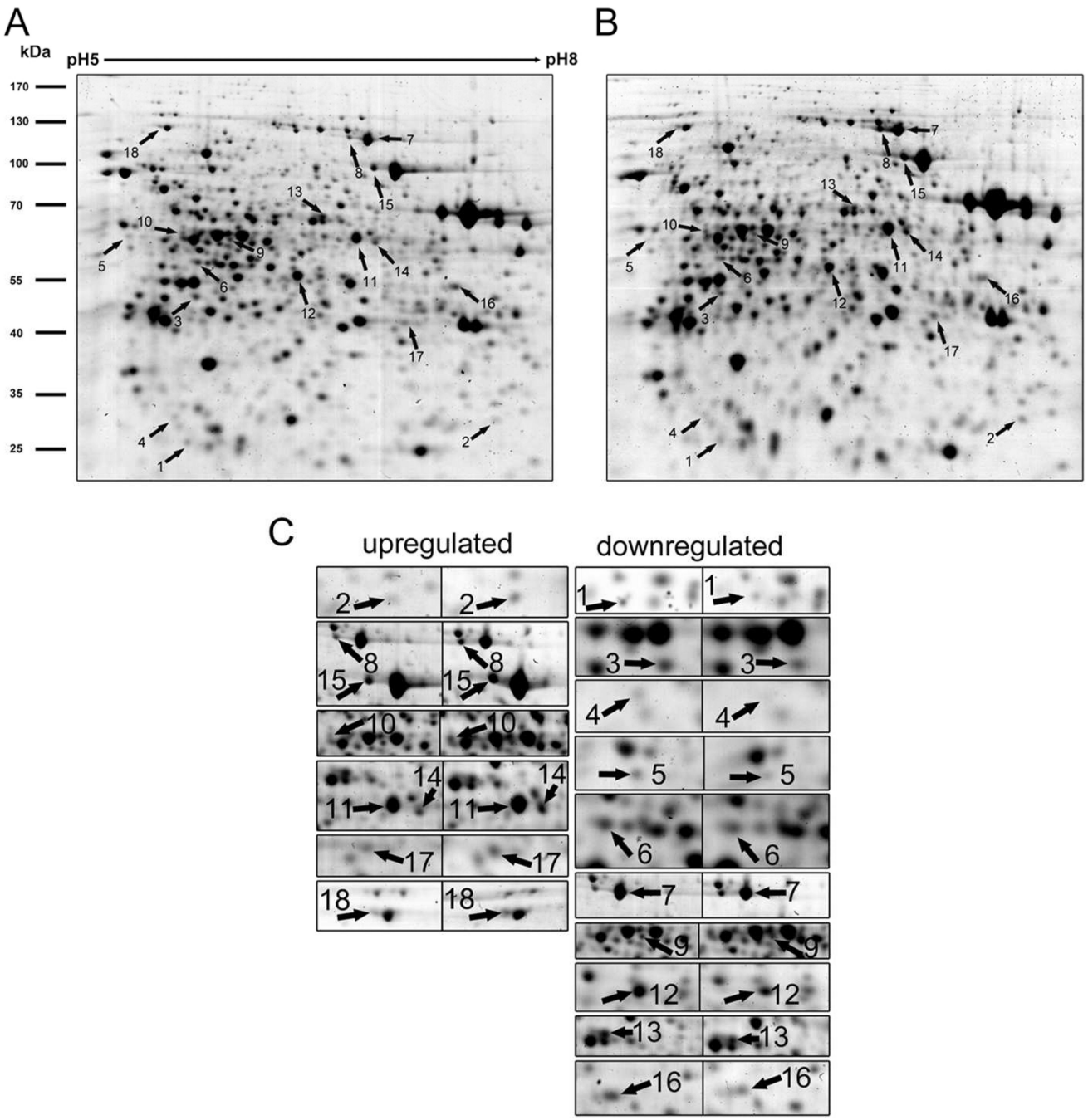

Figure 2.

Representative two dimensional gel of control (A) and LY294005 treated (B) Arabidopsis root protein extracts and details on individual spots (C) prepared from protein extract of LY294002 treated Arabidopsis roots. Proteins differentially abundant after LY294002 treatment are indicated by arrows. The numbers refer to proteins in Table 1

NIH-PA Author Manuscript
NIH-PA Author Manuscript
NIH-PA Author Manuscript

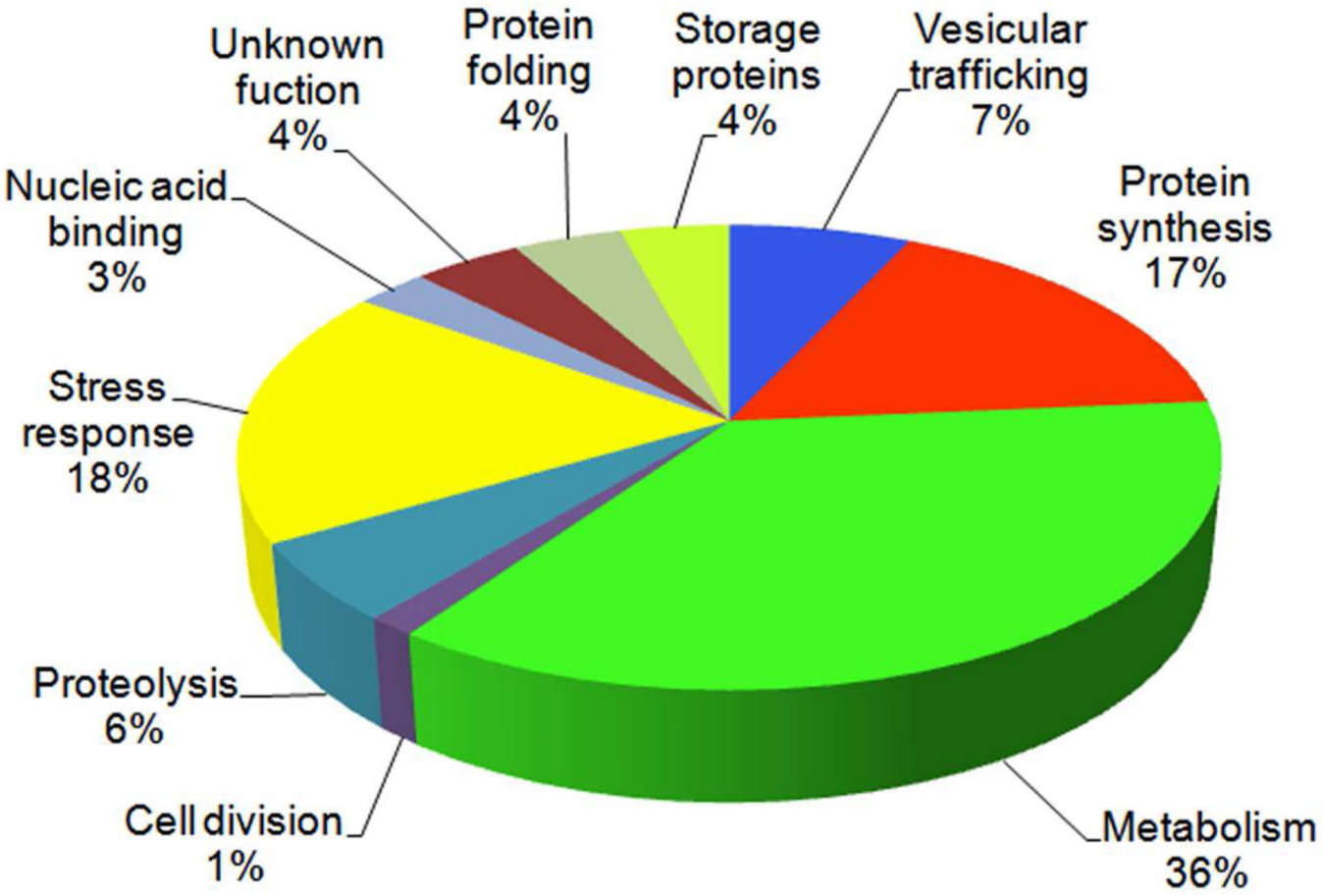

Figure 3.
Classification of the differentially abundant proteins into functional categories. The pie chart shows procentual distribution of proteins in diverse functional classes.

NIH-PA Author Manuscript

NIH-PA Author Manuscript

NIH-PA Author Manuscript

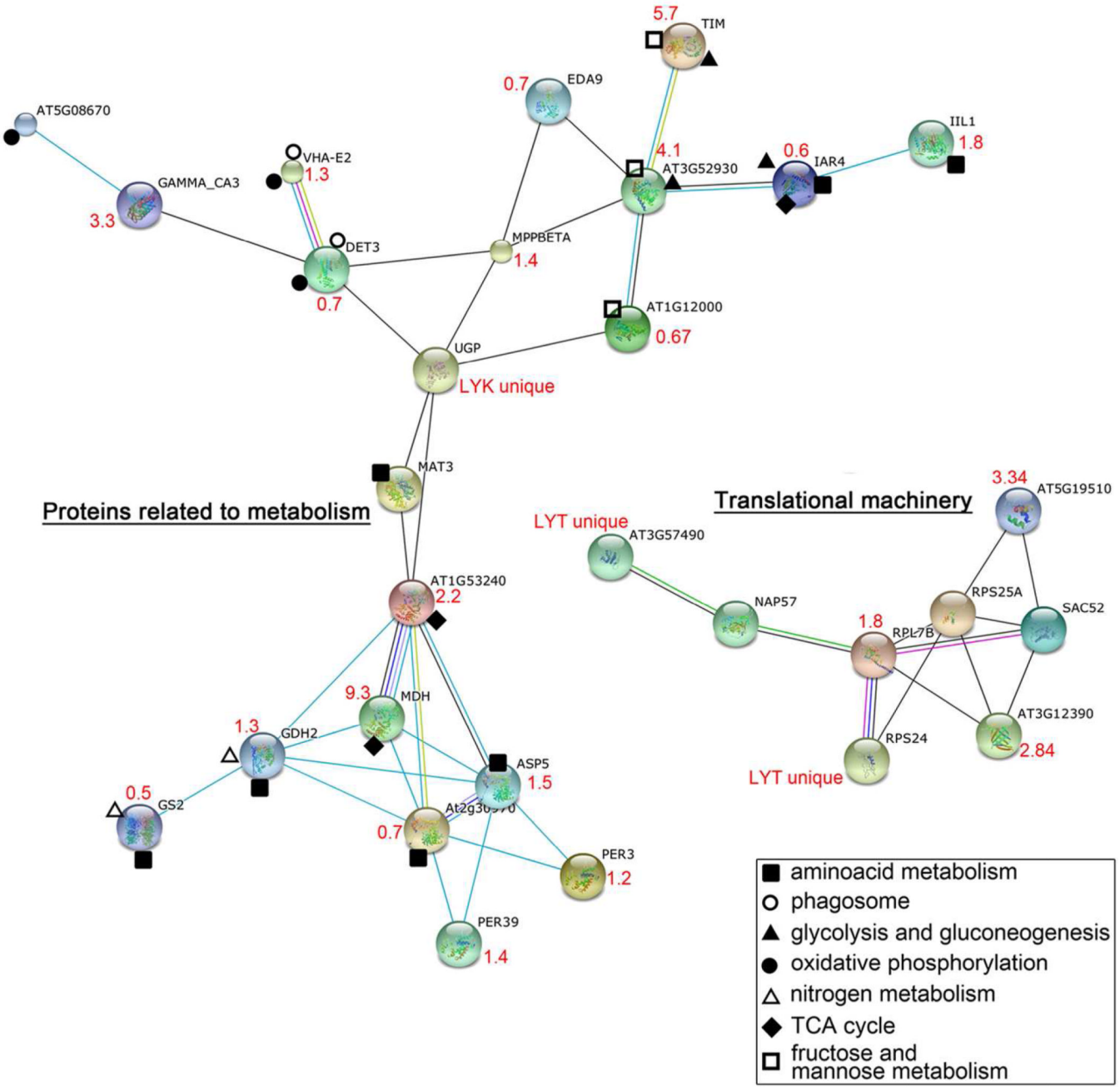

Figure 4.

Prediction of functional networks affected by LY294002 in Arabidopsis roots using STRING 9.0 applied on proteomic data. Different line colours represent the types of evidence used in predicting the associations: gene fusion (red), neighbourhood (green), co-occurrence across genomes (blue), co-expression (black), experimental (purple), association in curated databases (light blue) or co-mentioned in PubMed abstracts (yellow). The change in abundance (LY294002-treated vs control) of proteins is indicated in red. The single node proteins (those which do not interact) are not included in the figure. Explanation of abbreviations and accession numbers: TIM (triosephosphate isomerase); EDA9 (embryo sac development arrest 9); IAR4 (oxidoreductase), GAMMA CA3 (gamma carbonic anhydrase 3); DET3 (proton-transporting ATPase), MPPBETA (mitochondrial processing peptidase

NIH-PA Author Manuscript

NIH-PA Author Manuscript

NIH-PA Author Manuscript

beta subunit), AT3G52930 (fructose-bisphosphate aldolase, putative); IIL1 (isopropyl malate isomerase large subunit 1); UGP (UDP-glucose pyrophosphorylase); AT1G12000 (pyrophosphate--fructose-6-phosphate 1-phosphotransferase beta subunit, putative); AT1G53240 (malate dehydrogenase (NAD), mitochondrial); MDH (malate dehydrogenase); GDH2 (glutamate dehydrogenase 2); GS2 (glutamine synthetase 2); ASP5 (aspartate aminotransferase 5); At2g30970 (ASP1, aspartate aminotransferase 1); PER3 (RCI3, rare cold inducible gene 3); PER39 (peroxidase, putative); UNE5 (unfertilized embryo sac 5, protein disulfide isomerase); ATPDIL1–1 (PDI-like 1–1, protein disulfide isomerase); AT3G57490 (40S ribosomal protein S2, RPS2D); NAP57 (Arabidopsis thaliana homologue of NAP57, pseudouridine synthase); RPL7B (60S ribosomal protein L7, RPL7B); RPS25A (40S ribosomal protein S25 (RPS25B); AT5G19510 (elongation factor 1B alpha-subunit 2, eEF1Balpha2); SAC52 (suppressor of acaulis 52); AT3G12390 (nascent polypeptide associated complex alpha chain protein, putative); RPS24 (40S ribosomal protein S24, RPS24A).

NIH-PA Author Manuscript
NIH-PA Author Manuscript
NIH-PA Author Manuscript

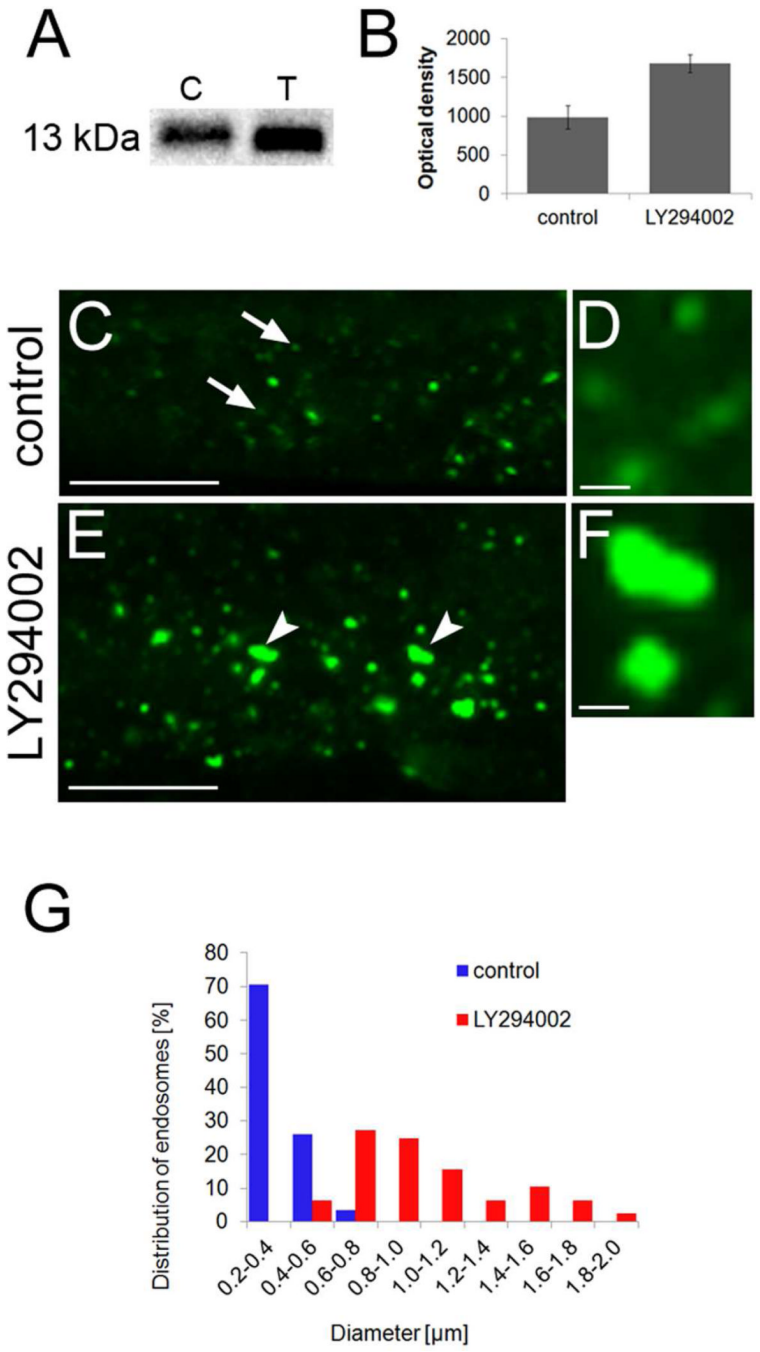

Figure 5.

Immunoblotting and immunolabeling analysis of 2S albumin in Arabidopsis roots after LY294002 treatment. A, Immunoblot detection of 2S albumin in control (C) and LY294002-treated (T) Arabidopsis roots. B, Quantification of optical density of bands corresponding to 2S albumin. Note that 2S albumin is more abundant after LY294002 treatment. C-F, Immunolabeling of 2S albumin in control (C, arrows and D) and LY294002-treated (E, arrowheads and F) Arabidopsis roots, G, Quantification of endosomal diameter in control and LY294002-treated root cells. Scale bars are 10μm for C, E, and 1 μm for D, F.

NIH-PA Author Manuscript
NIH-PA Author Manuscript
NIH-PA Author Manuscript

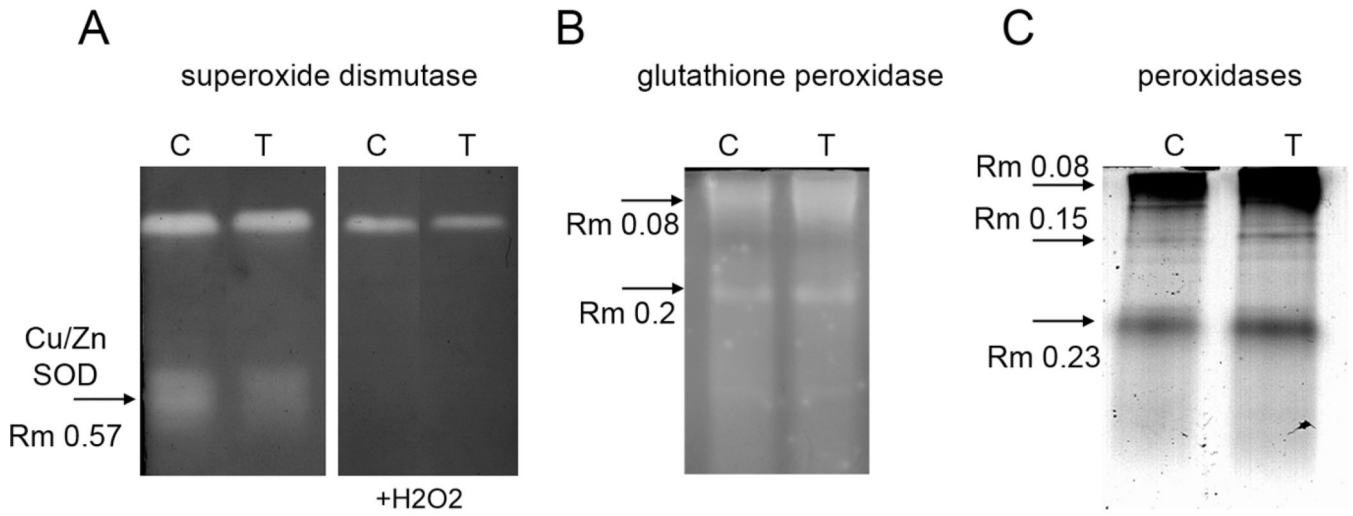

Figure 6.

Changes in isozyme pattern of selected antioxidant enzymes after treatment with LY294002 in native PAGE gels. A, Superoxide dismutase activity staining without H_2O_2 (left panel) and in the presence of H_2O_2 to identify Cu/ZnSOD isozyme. B, Glutathione peroxidase staining, C, Staining of peroxidases using 4-Cl-1-naftol as a substrate. Note decreased activity of Cu/ZnSOD (A) and increased activity of glutathione peroxidases and peroxidases after LY294002 treatment.

NIH-PA Author Manuscript

NIH-PA Author Manuscript

NIH-PA Author Manuscript

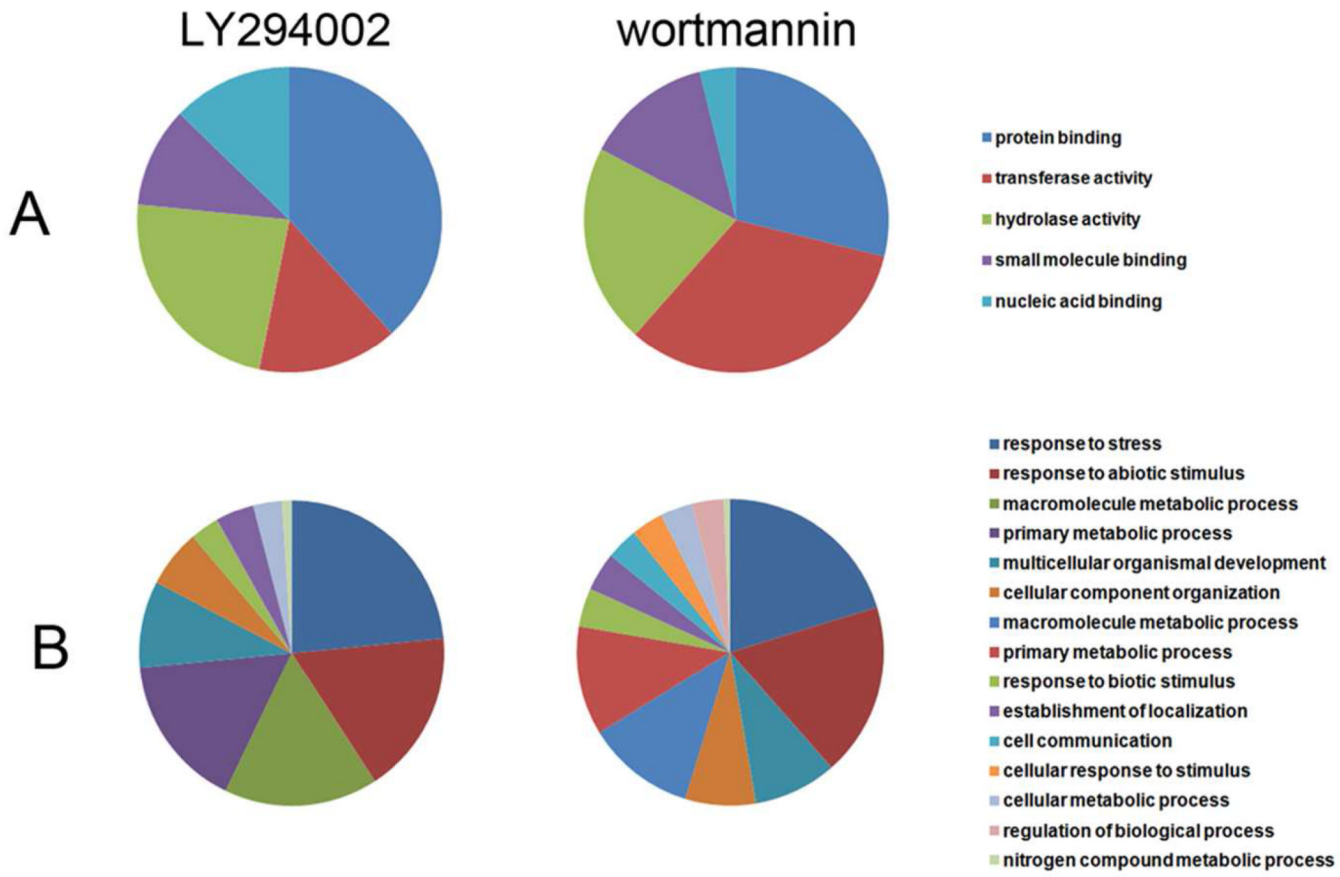

Figure 7.
Classification of differentially regulated proteins in Arabidopsis roots treated by LY294002 and wortmannin according to gene ontology annotations (Blast2GO application) for (A) biological process and (B) molecular function.

NIH-PA Author Manuscript
NIH-PA Author Manuscript
NIH-PA Author Manuscript

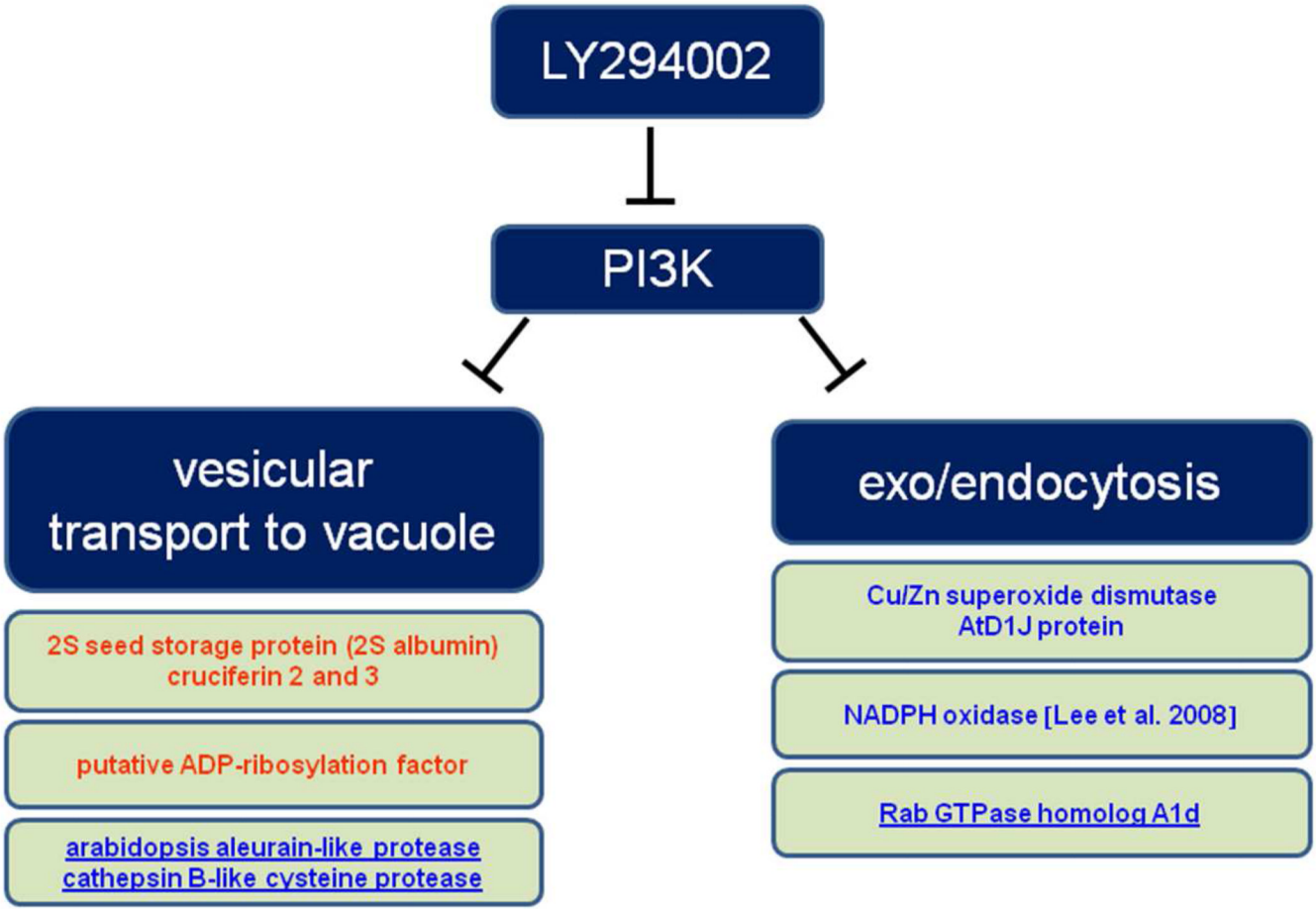

Figure 8.
Overview on proteins involved in vesicle-mediated vacuolar transport and endocytosis as identified by the present proteomic analysis using LY294002. Upregulated proteins are depicted in blue while downregulated ones are in red.

NIH-PA Author Manuscript NIH-PA Author Manuscript NIH-PA Author Manuscript

J Proteome Res. Author manuscript; available in PMC 2014 October 04.

Table 1

Proteins up- or downregulated by LY294002 in *Arabidopsis* roots.

Spot	Sequence ID	Sequence Name	Method of detection	Score[a]	Sequence Coverage (%)	Peptides identified	Total Spectral Count[b]	Mr theor/exp[c]	pI theor/ex	fold change[d]	ANOVA p-value
Vesicular trafficking											
1	NP_193615.1	Rab GTPase homolog A1d	2-D Gel	60.0	25.00	7		23.9/26.7	4.99/5.7	0.76	0.05
2	NP_187468.1	V-type proton ATPase subunit E2	2-D Gel	60.0	15	9		27.0/26.9	9.2/7.9	1.3	0.05
3	NP_563916.1	det3	2-D Gel	106.0	28.0	10		42.6/43.8	5.2/5.8	0.72	0.04
	NP_172533.2	ADP-ribosylation factor A1F	LC-MS/MS	3.9	27.6	2	3			LY294002 treated Unique	
	NP_191228.1	CAM interacting protein 111	LC-MS/MS	4.3	4.2	3	3			LY294002 treated Unique	
Protein synthesis											
	NP_191308.1	40S ribosomal protein S2 (RPS2D)	LC-MS/MS	8.6	14.1	3	3			LY294002 treated Unique	
	NP_187143.1	40S ribosomal protein S24 (RPS24A)	LC-MS/MS	2.9	9.0	1	6			LY294002 treated Unique	
4	NP 189421.1	50S ribosomal protein L12–1	2-D Gel	61.0	26	5		20.0/27.3	5.5/5.6	0.4	0.01
	NP_178234.1	60S ribosomal protein L7 (RPL7B)	LC-MS/MS	6.7	14.5	2	9			1.78	
	NP_563945.2	60S ribosomal protein L10 (RPL10A)	LC-MS/MS	8.9	21.8	4	18			1.43	
	NP_176134.1	XW6; structural constituent of ribosome	LC-MS/MS	9.7	22.9	4	6			LY294002 treated Unique	
5	NP_191274.1	H/ACA ribonucleoprotein complex subunit 4	2-D Gel	58.0	24.0	26		63.3/61.5	9.0/7.0	0.46	0.03
	NP_001031390.1	structural constituent of ribosome	LC-MS/MS	4.3	23.4	2	3			LY294002 treated Unique	
6	NP_566469.1	translational initiation factor 4A-1	2-D Gel	87.0	21	10		46.7/53.3	6.2/5.47	0.77	0.01
	NP_568375.2	elongation factor 1B alpha-subunit 2	LC-MS/MS	5.4	15.6	2	9			3.34	
7	AAF02837.1	elongation factor EF-2	2-D Gel	62	13	11		95.0/100.0	5.9/6.9	0.59	0.02

NIH-PA Author Manuscript
NIH-PA Author Manuscript
NIH-PA Author Manuscript

Spot	Sequence ID	Sequence Name	Method of detection	Score[a]	Sequence Coverage (%)	Peptides identified	Total Spectral Count[b]	Mr theor/exp[c]	pI theor/ex	fold change[d]	ANOVA p-value
Vesicular trafficking											
8	AAF02837.1	elongation factor EF-2	2-D Gel	62	13	11		95.0/102.7	5.9/6.8	2.1	0.05
Metabolism											
	NP_188048.1	pectin methylesterase 3	LC-MS/MS	5.5	8.1	2	3			LY294002 treated Unique	
	NP_186975.1	UDP-glucose pyrophosphorylase	LC-MS/MS	7.7	7.9	2	4			LY294002 control Unique	
	NP_195394.1	aminopeptidase P1	LC-MS/MS	8.4	4.3	2	4			LY294002 control Unique	
	NP_190336.1	malate dehydrogenase	LC-MS/MS	9.6	15.9	3	12			9.30	4.60E-5
	NP_564625.1	malate dehydrogenase (NAD), mitochondrial	LC-MS/MS	18.2	38.7	5	21			2.28	1.58E-2
	NP_188056.1	diaminopimelate decarboxylase, putative	LC-MS/MS	2.4	2.9	1	3			LYT LY294002 treated unique	
	NP_173828.1	IAA-conjugate-resistant 4	LC-MS/MS	8.9	14.8	4	24			0.66	1.39E-2
	NP_195131.1	caffeoyl-CoA 3-O-methyltransferase, putative	LC-MS/MS	9.2	29.7	4	9			2.10	1.40E-2
	NP_180654.1	aspartate aminotransferase 1	LC-MS/MS	6.2	14.0	3	19			0.69	5.99E-3
	NP_001031767.1	Aspartate aminotransferase 5	LC-MS/MS	7.7	9.5	2	13			1.50	1.77E-2
	NP_196361.1	glutamate dehydrogenase 2	LC-MS/MS	22.8	28.0	5	26			1.30	1.79E-2
	NP_001031969.1	glutamine synthetase 2	LC-MS/MS	7.8	11.4	2	16			0.46	2.48E-2
	NP_001031640.2	atard2; metal ion binding	LC-MS/MS	3.3	7.0	1	5			0.26	7.20E-3
	NP_195146.1	eda9 (embryo sac development arrest 9);	LC-MS/MS	16.9	18.2	5	23			0.72	2.53E-2
	NP_186858.1	metalloendopeptidase	LC-MS/MS	21.2	24.1	7	41			1.45	4.62E-2
	NP_179713.1	triosephosphate isomerase	LC-MS/MS	5.8	10.2	3	7			5.72	3.08E-2
	NP_001078808.1	gamma carbonic anhydrase 3	LC-MS/MS	4.5	7.8	2	5			3.34	3.24E-2
9	NP_568203.1	ATP synthase beta chain 1	2-D Gel	88.0	23	14		59.8/59.9	6.5/6.5	0.5	0.02
10	NP_568203.1	ATP synthase beta chain 1	2-D Gel	106.0	60	17		59.8/62	6.5/6.5	2.2	0.05

NIH-PA Author Manuscript
NIH-PA Author Manuscript
NIH-PA Author Manuscript

Spot	Sequence ID	Sequence Name	Method of detection	Score[a]	Sequence Coverage (%)	Peptides identified	Total Spectral Count[b]	Mr theor/exp[c]	pI theor/ex	fold change[d]	ANOVA p-value
Vesicular trafficking											
11	NP_085571	ATPase subunit 1	2-D Gel	66.0	19.00	12		54.98/59.8	6.2/6.9	1.34	0.02
12	NP_181225.1	S-adenosylmethionine synthase 3	2-D Gel	135.0	40	17		42.9/49.0	6.1/6.4	0.67	0.01
13	NP_172664.1	pyrophosphate--fructose-6-phosphate 1-phosphotransferase	2-D Gel	60.0	17	12		61.9/67.5	5.9/6.6	0.67	0.05
14	NP_567405.1	3-isopropylmalate dehydratase	2-D Gel	82.0	21.00	12		55.0/58.5	7.9/7.0	1.79	0.02
15	AAN31836.1	putative 5-methyltetrahydropteroyltriglutamate--homocysteine S-methyltransferase	2-D Gel	114.0	23	13		84.7/87.1	6.3/6.9	1.54	0.01
16	CAA11553.1	2-oxoglutarate dehydrogenase E2 subunit	2-D Gel	60.0	13.00	6		50.07/46.1	9.2/7.5	0.46	0.03
17	NP_190861.1	fructose-bisphosphate aldolase, class I	2-D Gel	109.0	32	16		38.8/38.0	6.0/7.1	4.1	0.03
Cell division											
18	|NP_187595	cell division control protein 48-A	2-D Gel	157.0	24.0	15		89.4/107.5	4.8/5.6	1.3	0.04
Proteolysis											
	NP_175158.1	20s proteasome alpha subunit f2	LC-MS/MS	4.2	17.7	2	3			LY294002 treated unique	
	NP_001077698.1	ubiquitin-specific protease 6	LC-MS/MS	4.0	3.4	1	3			LY294002 treated unique	
	NP_001032106.1	*Arabidopsis* aleurain-like protease	LC-MS/MS	12.2	16.0	2	24			0.69	2.89E-2
	NP_563648.1	cathepsin B-like cysteine protease	LC-MS/MS	9.6	18.5	4	16			0.55	8.00E-3
Stress response											
	NP_565666.1	copper/zinc superoxide dismutase 2	LC-MS/MS	7.1	26.9	2	9			0.46	9.02E-3
	NP_001031710.1	fe superoxide dismutase 1	LC-MS/MS	6.0	17.2	1	8			0.34	3.50E-2
	NP_001031791.1	catalase 2	LC-MS/MS	30.8	37.3	10	45			1.43	1.31E-2
	NP_192868.1	peroxidase, putative	LC-MS/MS	11.3	16.3	3	22			1.36	1.77E-2
	NP_192897.2	glutathione peroxidase 6	LC-MS/MS	9.2	14.7	2	6			4.10	1.01E-2
	NP_172018.1	rare cold inducible gene 3	LC-MS/MS	12.5	16.3	3	31			1.15	2.95E-2
	NP_001030698.1	class I glutamine amidotransferase domain-containing protein	LC-MS/MS	13.5	18.4	4	13			0.61	2.41E-2

NIH-PA Author Manuscript
NIH-PA Author Manuscript
NIH-PA Author Manuscript

Spot	Sequence ID	Sequence Name	Method of detection	Score[a]	Sequence Coverage (%)	Peptides identified	Total Spectral Count[b]	Mr theor/exp[c]	pI theor/ex	fold change[d]	ANOVA p-value
Vesicular trafficking											
	NP_568969.1	zinc finger (C2H2 type) family protein	LC-MS/MS	5.8	14.0	3	5			0.26	8.01E-3
	NP_176461.1	stress-inducible protein, putative	LC-MS/MS	12.3	14.5	4	5			LY294002 treated Unique	
	NP_178321.1	Low-molecular-weight cysteine-rich 68; protease inhibitor	LC-MS/MS	9.7	31.2	2	29			0.79	2.93E-2
	NP_195271.2	NADPH-dependent thioredoxin reductase 1	LC-MS/MS	8.7	14.1	3	8			0.52	2.45E-2
	NP_001030710.1	PYK10-binding protein 1	LC-MS/MS	72.5	78.2	17	232			0.90	3.80E-2
	NP_189276.1	major latex protein-related	LC-MS/MS	9.5	27.0	2	9			1.97	1.28E-2
Nucleic acid binding											
	NP_188431.3	HON4; DNA binding	LC-MS/MS	3.4	3.8	1	7			2.24	1.71E-2
	NP_179760.1	ATGRP7	LC-MS/MS	11.3	27.3	4	15			2.65	3.25E-2
Storage proteins											
	NP_194581.1	cruciferin 3	LC-MS/MS	36.9	36.8	11	25			LY294002 treated Unique	
	NP_171884.1	cruciferin 2	LC-MS/MS	16.7	24.4	6	9			LY294002 treated Unique	
	NP_194445.1	2S seed storage protein 2	LC-MS/MS	5.7	15.3	2	4			LY294002 treated Unique	
Protein folding											
	NP_001031555.1	PDI-LIKE 2–1	LC-MS/MS	8.9	23.8	3	5			3.80	8.12E-3
	NP_173594.1	PDI-LIKE 1–1	LC-MS/MS	21.7	23.2	7	39			1.65	8.12E-3
	NP_198206.1	luminal binding protein 1	LC-MS/MS	29.3	18.8	9	54			1.59	2.59E-2
Unknown function											
	NP_187845.1	nascent polypeptide associated complex alpha chain protein, putative	LC-MS/MS	6.1	11.8	2	8			2.84	2.73E-2
	NP_565497.3	rhodanese-like domain-containing protein	LC-MS/MS	6.1	16.6	2	4			LY294002 treated	
										Unique	

NIH-PA Author Manuscript
NIH-PA Author Manuscript
NIH-PA Author Manuscript

Spot	Sequence ID	Sequence Name	Method of detection	Score[a]	Sequence Coverage (%)	Peptides identified	Total Spectral Count[b]	Mr theor/exp[c]	pI theor/ex	fold change[d]	ANOVA p-value
Vesicular trafficking											
	NP 196647.1	CBS domain-containing protein	LC-MS/MS	6.6	13.6	1	7			0.36	6.60E-3
	NP_565791.1	katanin, putative	LC-MS/MS	3.2	4.7	1	3			LY294002 control Unique	

a) MOWSE score of Mascot algorithm for 2-D Gel MALDI TOF-TOF; Summ of Xcorr of TURBOSEQUEST algorithm for 2- D LC ESI MSMS

b) given and significant only for 2-D LC ESI MSMS

c) given and significant only for 2-D Gel MALDI TOF-TOF

d) based on spot intensity for 2-D Gel MALDI TOF-TOF; based on normalized average spectral count for 2- D LC ESI MSMS

J Proteome Res. Author manuscript; available in PMC 2014 October 04.

NIH-PA Author Manuscript
NIH-PA Author Manuscript
NIH-PA Author Manuscript

Table 2

The relative optical densities of native PAGE bands stained for Cu/Zn superoxide dismutase (SOD), glutathione peroxidase (GPX) and peroxidase (POX) activities. Data for LY294002 are presented as an average of 3 biological replicates (± standard deviation).

	Cu/ZnSOD	GPX		POX		
band	Rm 0.57	Rm 0.08	Rm 0.2	Rm 0.08	Rm 0.15	Rm 0.23
DMSO	100	100	100	100	100	100
LY294002	77±9.8	120.3±5.0	122.7±5.1	131±5.1	455±25.1	119±6.6

J Proteome Res. Author manuscript; available in PMC 2014 October 04.

NIH-PA Author Manuscript

NIH-PA Author Manuscript

NIH-PA Author Manuscript

Table 3

List of proteins differentially affected by LY294002 and wortmannnin. Equally differentially regulated proteins are indicated by bold text.

Functional class	Sequence ID	Sequence Name	Fold change	
			LY294002	wortmannin
Vesicular trafficking	**NP193615.1**	**Rab GTPase homolog A1d**	**0.70**	**0.59**
	NP 563916.1	**det3**	**0.72**	**0.86**
	NP563648.1	**cathepsin B-like cysteine protease**	**0.55**	**0.27**
	NP 001032106.1	***Arabidopsis* aleurain-like protease**	**0.69**	**0.75**
metabolism	**NP181225.1**	**S-adenosylmethionine synthase 3**	**0.67**	**0.55**
	NP 567405.1	**3-isopropylmalate dehydratase**	**1.79**	**1.34**
cell division	**NP 187595**	**cell division control protein 48-A**	**1.3**	**1.52**
metabolism	NP 186975.1	UDP-glucose pyrophosphorylase	LYK Unique	2.46
nitrogen	NP 196361.1	glutamate dehydrogenase 2	1.30	0.65
metabolism	NP 001031969.1	glutamine synthetase 2	0.46	3.27
protein transport (mitochondria)	NP 186858.1	metalloendopeptidase	1.45	0.7
stress response	NP 001031710.1	fe superoxide dismutase 1	0.34	2.17
	NP 192868.1	peroxidase, putative	1.36	0.33
	NP 172018.1	rare cold inducible gene 3	1.15	0.44
	NP 189276.1	major latex protein-related	1.97	0.37
protein folding	NP 198206.1	luminal binding protein 1	1.59	0.47